Research Square

Preprints are preliminary reports that have not undergone peer review.
They should not be considered conclusive, used to inform clinical practice,
or referenced by the media as validated information.

Individual plant-level (IPL) soybean biomass estimation and spatial mapping through UAV multisource feature-driven machine learning framework

Gyujin Jang
Seoul National University
Yuna Kwon
Seoul National University
Yong-Hyun Kim
Seoul National University
Yong-Suk Chung
Jeju National University
Won Suk Lee
University of Florida
Hak-Jin Kim
kimhj69@snu.ac.kr

Seoul National University

Research Article

Keywords: Feature fusion, Plant phenotyping, Precision agriculture, Remote sensing, Spatial variability

Posted Date: June 10th, 2026

DOI: https://doi.org/10.21203/rs.3.rs-9879825/v1

License: This work is licensed under a Creative Commons Attribution 4.0 International License.
Read Full License

Additional Declarations: No competing interests reported.

Individual plant-level (IPL) soybean biomass estimation and spatial mapping through UAV multisource feature-driven machine learning framework

Gyujin Jang[1,2*], Yuna-Kwon[1,2], Yong-Hyun Kim[1,2], Yong-Suk Chung[3] Won Suk Lee[5] and Hak-Jin Kim[1,5,6*]

[1] Department of Biosystems Engineering, Seoul National University, Seoul 08826, Republic of Korea
[2] Integrated Major in Global Smart Farm, Seoul National University, Seoul 08826, Republic of Korea
[3] Department of Plant Resources and Environment, Jeju National University, Jeju 63243, Republic of Korea
[4] BrainKorea21 Global Smart Farm Educational Research Center, Seoul National University, Seoul 08826, Republic of Korea
[5] Department of Agricultural & Biological Engineering, University of Florida, Gainesville, FL 32611, USA
[6] Research Institute of Agriculture and Life Sciences, Seoul National University, Seoul 08826 Republic of Korea
kimhj69@snu.ac.kr

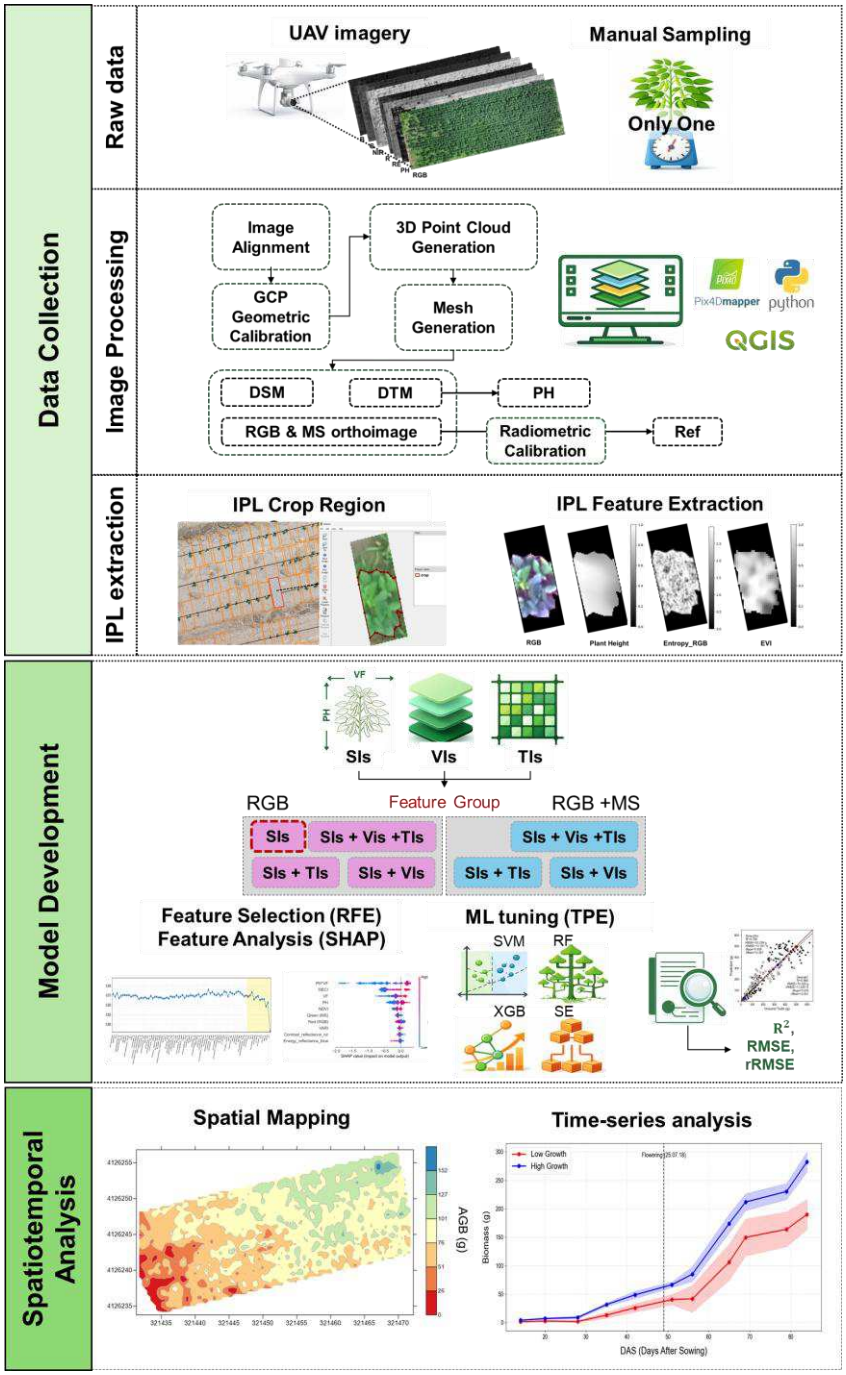
Abstract

Rapid and accurate quantification of crop biomass using multisource UAV imagery–derived features, such as plant height, vegetation indices, and texture indices demonstrates strong potential for soybean high-throughput phenotyping. The indeterminate growth habit of soybean, alongside extensive nodulation and intense inter-plant competition, necessitates individual plant level (IPL) monitoring to quantify plant-specific nitrogen fixation and competitive vigor. However, most studies aggregate measurements at multi-plants at the plot level, thereby masking these soybean-specific traits. This study aims to develop and evaluate a UAV imagery-based framework for estimating soybean biomass at the IPL, with the objective of characterizing high-resolution spatial variability and supporting high-throughput phenotyping.

Regions of interest (ROIs) for IPL data acquisition were defined as rectangular plots based on planting density and were generated from early-stage imagery before canopy overlap occurred. Using these ROIs, structural information (SIs) including plant height (PH) and vegetation fraction (VF)), vegetation indices (VIs), and texture indices (TIs) were derived for each individual plant from RGB and multispectral imagery and organized into sensor-specific feature groups. Recursive feature elimination was applied to select optimal features, which were then used as inputs for machine learning architectures including support vector regression (SVR) with a linear kernel, Random Forest (RF), and XGBoost (XGB). Among them, the SVR model using fused multisource features (SIs + VIs + Tis) achieved the best performance, with $R^2 = 0.88$, RMSE = 55.34 g, and rRMSE = 8.50% on an independent test dataset. The results show that: (1) tree-based models, including XGB and RF may suffer from overfitting due to limited sample size and feature redundancy, whereas linear SVR showed better generalization; (2) fusing RGB and multispectral features consistently improved biomass estimation accuracy. Inparticular, near-infrared and red-edge-based indices such as RECI and NDRE, along with VF and PH, were identified as important predictors, while texture indices were not selected as significant features; and (3) the proposed framework enabled spatially explicit IPL biomass mapping and time-series analysis, revealing variability in growth conditions and distinct growth trajectories. The framework provides a reliable solution for IPL soybean biomass estimation with practical potential for UAV-based agricultural decision-making.

Keywords: Feature fusion; Plant phenotyping; Precision agriculture; Remote sensing; Spatial variability

Graphical abstract



Highlights

- UAV multisource imagery including RGB and multispectral enables individual plant level soybean biomass estimation
- SVR model with fusing multisource features achieved highest accuracy (R^2 = 0.89)
- Multispectral imagery-based features—near-infrared and red-edge-based indices such as Red Edge Chlorophyll Index and Normalized Difference Red Edge—improved biomass prediction performance beyond RGB imagery-based features such as VF and PH.
- Spatiotemporal IPL analyses demonstrate the feasibility of biomass estimation by capturing spatial patterns and growth dynamics.

1 Introduction

Soybean (*Glycine max* L.) is a major global food crop and leading plant-based protein source, playing a critical role in food security (Hartman et al., 2011). In recent decades, the increasing frequency of extreme climatic events associated with global climate change has posed significant challenges to soybean productivity and quality (Mall et al., 2004). These challenges have driven intensive breeding efforts to develop cultivars with enhanced adaptability and stable yields (Thomasz et al., 2024). Biomass is a key physiological trait that reflects crop vigor and growth potential, encompassing factors such as photosynthetic efficiency, light interception, and competitive ability against weeds (Hsiao et al., 2009; Huang et al., 2016; Oerke, 2006). However, traditional manual biomass measurements are destructive, labor-intensive, and inefficient for large-scale phenotyping (Ubbens et al., 2020). Unmanned aerial vehicle (UAV)-based remote sensing provides a non-destructive, cost-effective, and faster alternative that enables high-throughput acquisition of spatially explicit data (Jang et al., 2020; Zambrano et al., 2023). Therefore, integrating UAV imagery into soybean biomass estimation represents a promising approach to improve efficiency and precision in field breeding programs (Kouadio et al., 2023; Liu et al., 2025; Tanaka et al., 2024)

Soybean exhibits indeterminate growth and continuously reallocates biomass throughout its growth period. Root nodulation varies among individual plants due to the spatial heterogeneity of rhizobial populations, leading to differences in nitrogen fixation capacity (López-García et al., 2002). In addition, substantial plant-to-plant variability in growth and yield occurs, and can be further influenced by planting density and stand uniformity, ultimately contributing to significant variation in biomass among individual plants (Masino et al., 2018; Purcell et al., 2002). Thus, assessing biomass at the individual plant level (IPL) enables a more accurate characterization of growth

dynamics and plant-to-plant interactions, thereby supporting the precise identification and selection of high-performing, resilient genotypes.

However, in most UAV imagery–based soybean growth prediction studies, biomass datasets are typically constructed by defining regions of interest (ROIs) that encompass multiple plants. UAV-derived image features within each ROI are aggregated to generate representative values and paired with corresponding ground-measured mean biomass to develop machine learing-based models (Da et al., 2025; Okada et al., 2024; Ranđelović et al., 2023). Therefore, this study aims to address this research gap by evaluating the feasibility of UAV-based IPL soybean biomass estimation, a topic that remains underexplored.

Among the various sensing modalities used in UAV-based phenotyping, RGB imagery enables the extraction of structural information (SIs) related to crop canopy volume, including vegetation fraction (VF) and plant height (PH) (Bendig et al., 2014; Kim et al., 2018, 2023). These UAV-derived SIs show strong potential for predicting crop biomass. For example, Kim et al. (2018) and Kim et al. (2023) developed linear regression models using VF and PH derived from RGB imagery, achieving strong predictive performance for radish and Chinese cabbage, and for onion and garlic, respectively. However, beyond crop volume, traits related to tissue composition, such as epidermal and mesophyll structures, influence mass density and spatial morphology, both of which closely correlate with biomass (Ye et al., 2024; Zhao et al., 2023). Therefore, several studies incorporated vegetation indices (VIs) and texture indices (TIs) derived from gray-level co-occurrence matrix (GLCM) analysis (Matyukira & Mhangara, 2024; Yang et al., 2025). These VIs and TIs improve prediction accuracy when integrated with structural features. However, RGB imagery alone has inherent limitations, as it primarily captures canopy structure and visible reflectance. In contrast, VIs and TIs derived from near-infrared (NIR) and red-edge spectral bands provide additional information on crop

physiological characteristics and plant health (Biswal et al., 2024a; Liu et al., 2025). Therefore, fusing multisource UAV data from RGB and multispectral sensors has the potential to provide more comprehensive information on crop biomass. However, there are not many studies that systematically integrate multisource UAV data for IPL crop biomass prediction. Understanding the contributions and predictive performance of features derived from different sensors is essential for the effective application of UAV-based remote sensing in practical phenotyping systems.

Deep learning models have received increasing attention for estimating crop growth from UAV imagery (Ali et al., 2025; Malashin et al., 2024). Deep learning–based image regression models automatically extract features relevant to crop growth and achieve high prediction accuracy when large training datasets are available. In contrast, machine learning (ML) approaches based on explicit feature extraction are widely used for biomass estimation because they provide high interpretability and perform reliably when training data are limited (Da et al., 2025a; Okada et al., 2024). Since fused multisource features typically comprise numerous input variables, ML models are well-suited to high-dimensional feature spaces and effectively capture complex relationships among variables, thereby enabling robust predictive performance in soybean biomass estimation. (Da et al., 2025a; Ranđelović et al., 2023; Shammi et al., 2025; Zhu et al., 2025). Several studies have compared the performance of different ML architectures for estimation; however, they did not strictly separate calibration and test datasets across different cultivation environments. Such experimental designs can lead to optimistic performance estimates and hinder accurate evaluation of model generalization. In agricultural applications, where datasets are inherently limited, it is essential to develop machine learning-based models that mitigate overfitting and ensure robust generalization (Liu et al., 2025).

For IPL soybean biomass estimation, this study proposes a framework based on multisource UAV imagery including RGB and multispectral data. The specific objectives are: (1) to develop and evaluate machine learning models for IPL soybean biomass prediction; (2) to investigate the contributions of multisource UAV imagery to biomass estimation; and (3) to explore the feasibility of applying the proposed framework to high-throughput phenotyping.

To achieve these objectives, the performance of various ML architectures was systematically evaluated, and model robustness was assessed using soybean datasets collected under diverse environmental conditions. This study further explored SI-based biomass estimation by incorporating RGB-derived VIs and TIs, alongside features from multispectral imagery. In addition, spatiotemporal analysis of IPL soybean biomass was conducted to demonstrate the applicability of the proposed framework. Specifically, the feasibility of the approach was validated by comparing biomass maps generated at the IPL with those at plot-level spatial resolution, while generating growth curves relevant to growers.

2 Materials and Methods

2.1 Test field and biomass collection

A two-year field experiment was conducted in two separate soybean (*Glycine max (L.) Merrill*) fields during the 2024 and 2025 growing seasons, from June to September. UAV-based imaging was carried out at the University Farm of Seoul National University (37° 15′ 54.85″ N, 126° 59′ 22.13″ E, altitude 35 m), located in Suwon, Republic of Korea (Fig. 1). At the experimental site, the average temperatures during the 2024 and 2025

growing seasons were 27.1 °C and 26.5 °C, respectively, while total rainfall amounted to 183.0 mm and 490.0 mm, respectively.

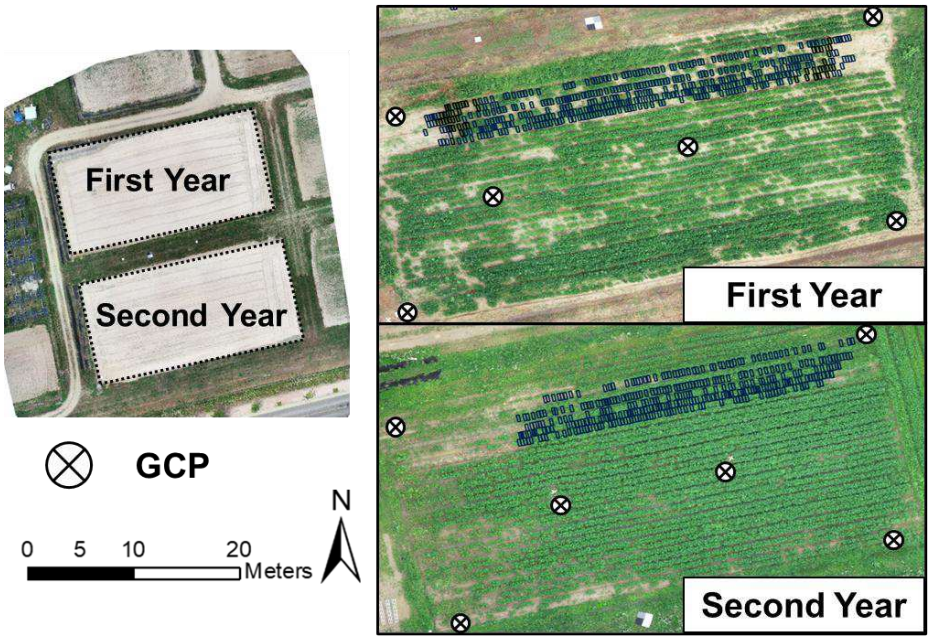


Fig. 1. Test sites during the 2024 and 2025 soybean growing seasons. Data from 2024 were used for model development, while data from 2025 were used for validation under different environmental conditions. Soybeans were sown using a mechanical seed drill, with row and interplant spacing of 65 × 24 cm in 2024 and 60 × 24 cm in 2025.

Data collected in 2024 were used to develop a multisource UAV-based machine learning framework for IPL soybean biomass estimation, whereas data collected in 2025 were used to validate the developed models under different environmental conditions. In both years, soybeans were sown using a mechanical soybean seed drill (Jang Seeder, Korea). During west-to-east sowing, a tractor-mounted system performed rotary tillage, ridge formation, and seeding in a single pass, with each row initiated from the western region

and completed toward the east, and operations repeatedly restarting from the west for subsequent rows. Row spacing and interplant spacing were set, respectively, to 65 cm and 24 cm in 2024, and to 60 cm and 24 cm in 2025. Approximately ten days after germination, thinning was conducted to retain a single plant per hole where multiple seedlings had emerged. In 2024, all plots were planted with the soybean cultivar *Gwanak1 (Glycine max (L.) Merrill)*, whereas in 2025, an additional cultivar, *Seonyu2ho (Glycine max (L.) Merrill)*, was planted.

Plant biomass was determined by destructive sampling, in which roots were removed, and the fresh weight of each plant was measured individually immediately after sampling. To develop a generalized model capable of estimating biomass during periods of active soybean growth, samples were collected up to the pod formation stage, when substantial increases in biomass typically occur. Growth stages were identified according to the Biologische Bundesanstalt, Bundessortenamt und Chemische Industrie (BBCH) scale (LANCASHIRE et al., 1991) as summarized in Table A1. In addition, the growing degree days (GDD) for each observation date were calculated following the procedures in (Alsajri et al., 2019). In 2024, 410 samples of the cultivar *Gwanak1* were collected. In 2025, 240 samples of *Gwanak1* and 230 samples of *Seonyu2ho* were collected.

2.2 Workflow design

Fig. 2 shows that the biomass estimation algorithm followed the workflow. First, UAV platforms equipped with RGB and multispectral cameras were used to acquire imagery. The raw images were processed to generate reflectance-aligned mosaics and three-dimensional point cloud-based plant height (PH) products. For surveyed plants, IPL ROIs were defined based on sowing density, and crop regions were subsequently segmented.

For each IPL crop region, features were extracted and grouped by sensor type: RGB-only or RGB combined with multispectral imagery. Each feature group included structural information (SIs) as the primary predictors for biomass estimation, along with vegetation indices (VIs) and texture indices (TIs). Based on these datasets, recursive feature elimination (RFE) was applied across four machine learning architectures to identify optimal feature combinations and develop the best-performing model for each feature group. Finally, features extracted from crop regions in the test dataset were input into the biomass estimation models developed during the training stage.

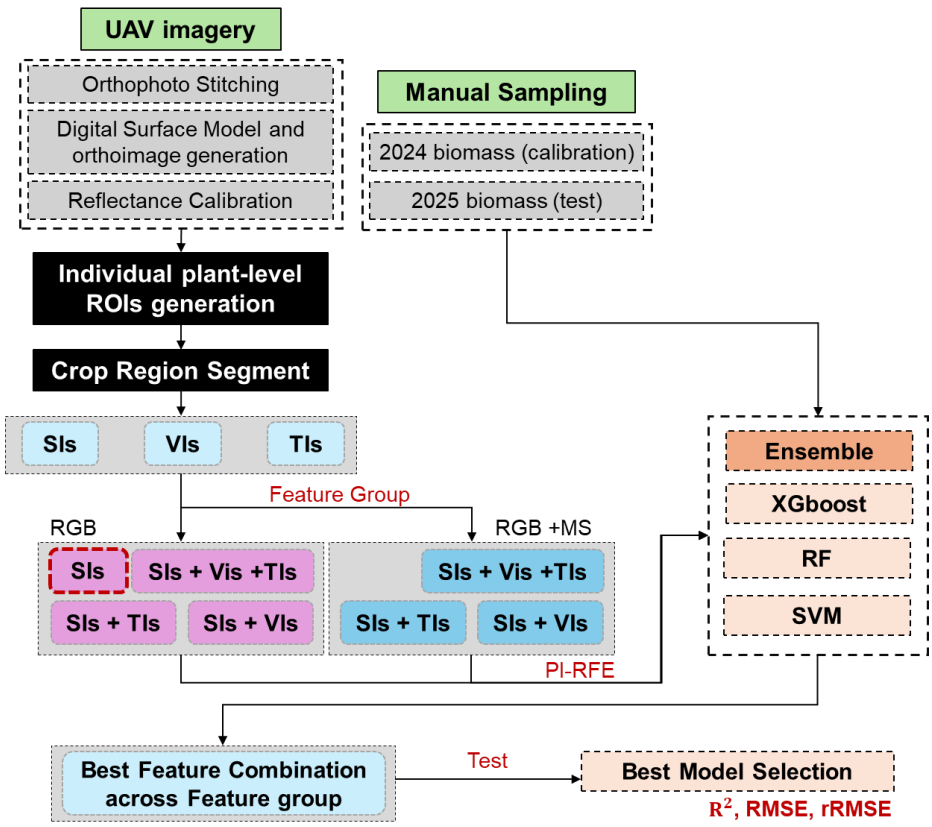


Fig. 2. Workflow of soybean biomass estimation model development. SI, VI, and TI denote structural information, vegetation indices, and texture indices, respectively

2.3 Data collection

2.3.1 UAV flight and image acquisition

RGB imagery was acquired using a DJI Phantom 4 Pro V2.0 (DJI, Shenzhen, China), equipped with a 1-inch CMOS sensor, capturing visible bands (blue, green, and red) at a resolution of 5472 × 3648 pixels. Multispectral imagery was collected using a DJI P4 Multispectral camera (DJI, Shenzhen, China), which captures five spectral bands: blue (450 ± 16 nm), green (560 ± 16 nm), red (650 ± 16 nm), red edge (730 ± 16 nm), and near-infrared (840 ± 26 nm) at 1600 × 1300 pixels

The UAV flights were conducted at an altitude of 20 m using the GS Pro application (DJI, China), with 85% forward and side overlap to ensure complete coverage of the study area. All flights were conducted between 10:00 and 13:00 local time under stable illumination conditions. A summary of UAV flights and biomass sampling dates during the 2024 and 2025 growing seasons is provided in Table A1.

2.3.2 Image preprocessing

The acquired UAV imagery was processed using photogrammetry software (Pix4Dmapper 3.1.7, Pix4D SA, Switzerland) based on the Structure from Motion (SfM) algorithm to generate orthomosaic images and a three-dimensional digital surface model (DSM). Through this process, RGB orthomosaics, band-specific multispectral mosaics, and DSMs were obtained.

To improve the spatial accuracy of the UAV-derived imagery, six ground control points (GCPs) were installed in the test field using aluminum panels painted black and white (Fig, 1). Their coordinates were measured using a real-time kinematic global positioning system (RTK-GPS, Model No. C099-F9P) with vertical and horizontal accuracy within 10 cm, and these data were used for geometric correction.

To minimize the influence of varying light and atmospheric conditions on UAV images captured at different times, radiometric calibration was performed for each flight. During each mission, 0.6 × 0.6 m Group 8 Technology Type 822 calibration panels with four grayscale reflectance levels (3%, 11%, 33%, and 55%) were placed within the UAV flight path. For RGB imagery, empirical line calibration was applied (Yun et al., 2016), while for multispectral imagery, a linear calibration relationship was applied using standard calibration panels (Wang et al., 2024).

2.3.3 IPL multisource imagery extraction

In this study, UAV-based multisource imagery data were obtained for IPL crops (Fig. 3). RGB orthomosaic images acquired at the early growth stage were first employed to determine individual plant centroids (June 21, 2024, 13 days after sowing; and June 13, 2025, 13 days after sowing; Table A1). At this stage, soybean plants did not overlap, allowing individual plant centroids to be reliably identified. Because these initial centroids remained spatially stable unless plants were physically removed, ROIs were generated based on these reference points. The centroids were manually annotated (red dots in Fig. 3a).

To reflect planting density, each ROI in 2024 was defined as a rectangle measuring 65 cm along the planting rows (vertical direction) and 24 cm between plants within a row (horizontal direction), as shown in orange rectangles in Fig. 3a. In 2025, the corresponding dimensions were 60 cm and 24 cm for vertical and horizontal directions, respectively. To determine the orientation of each ROI, crop row centerlines were manually delineated, and the rectangles were aligned with these row directions, as shown in black lines in Fig. 3a. The generated ROIs served as spatial units for extracting UAV-based multisource imagery at ground-sampled locations. The ROI generation

295 in Fig. 3a was conducted using QGIS Desktop 3.26.2 (QGIS Development
296 Team).
297 Background elements, including weeds and soil, were removed from the
298 UAV-based multisource images extracted for each ROI to enable feature
299 extraction exclusively from crop regions. Crop areas were manually
300 delineated using polygon annotations (Fig. 3b). The open-source tool Labelme
301 was used to label crop regions based on RGB imagery for all samples,
302 generating annotation files in JSON format. These annotations were
303 subsequently converted into binary PNG masks, in which crop pixels were
304 assigned a value of 1 and background pixels a value of 0. The resulting masks
305 were used as crop-only regions for feature extraction within each IPL ROI.
306

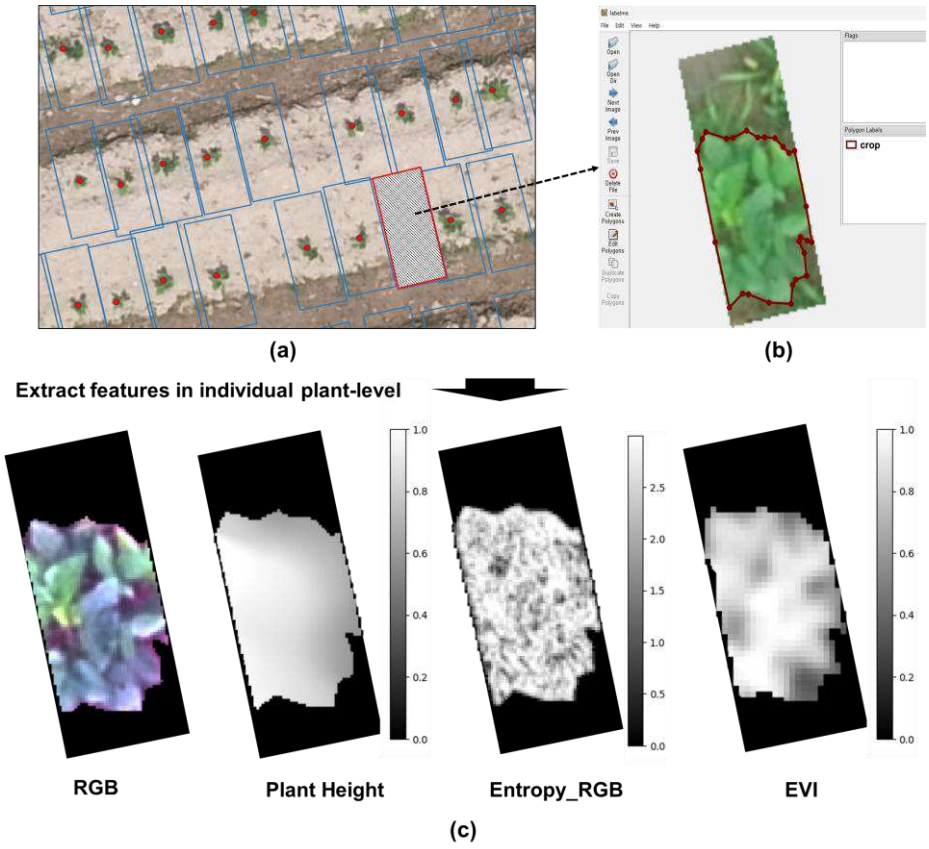


Fig. 3. IPL feature extraction procedure: (a) generated IPL ROIs (orange rectangles), where white dots indicate crop centroids at the early growth stage and black lines represent crop rows; (b) generating crop region annotations for each sampled ROI using Labelme; (c) extracted features from the sample shown in (b), including radiometrically calibrated RGB imagery, plant height, texture indices (e.g., Entropy from RGB), and vegetation indices (e.g., EVI).

2.3.4 UAV multisource feature dataset configuration

The extracted features included structural information (SIs), vegetation indices (VIs), and texture indices (TIs). The SIs consisted of PH, vegetation fraction (VF), and PH × VF, which represents crop volume. PH was determined as the maximum value obtained by subtracting the digital terrain model (DTM) generated before crop emergence from the digital surface

model (DSM) generated after crop emergence (Fig. 4). The crop height predicted using the proposed method showed the estimation performance presented in Fig. A1. In this study, RGB images acquired using the DJI Phantom 4 Pro V2.0 were compared with ow-resolution RGB images (1600 × 1300) from the DJI P4 Multispectral. The high-resolution RGB images provided noticeably improved prediction performance, showing higher R^2 values and lower RMSE values than the low-resolution RGB images. Therefore, to ensure reliable crop height estimation, two separate UAV flights were conducted in this study, as described in Section 2.3.1. VF was calculated by dividing the number of pixels within the generated crop region by the total number of pixels within the ROI.

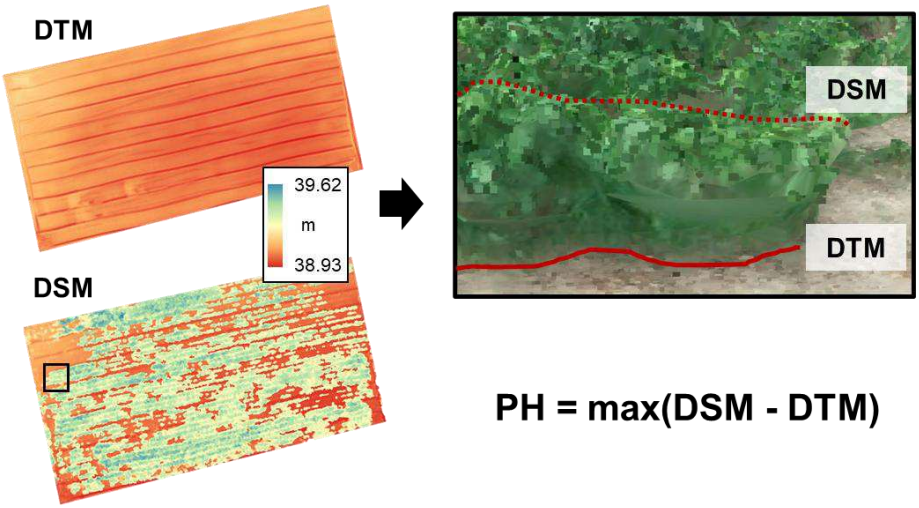


Fig. 4. Estimation of plant height (PH) from structure-from-motion (SfM)–derived point clouds, using the difference between the digital surface model (DSM) and digital terrain model (DTM). The DSM represents the crop canopy surface (red dashed line), while the DTM corresponds to the ground surface in the absence of vegetation (red solid line)

For the RGB imagery, VIs were derived from the R, G, and B bands, and TIs were calculated from grayscale-converted images and plant height (PH) images. For multispectral imagery, VIs were computed using bands including near-infrared (NIR) and red-edge, and TIs were obtained from all five spectral bands.

A total of 12 VIs were calculated for RGB imagery, while 15 VIs were derived from multispectral imagery. All indices were computed based on surface reflectance values. The formulas and descriptions of these VIs are presented in Tables A2and A3, which include difference-based, ratio-based, normalized, and composite index approaches. Representative example of EVI is illustrated in Fig. 3.

Texture indices were extracted using the grey-level co-occurrence matrix (GLCM) from grayscale-converted RGB images, PH maps, and five multispectral bands (R, G, B, red-edge, and NIR). Six texture metrics (homogeneity, contrast, dissimilarity, entropy, energy, and correlation) were computed, which resulted in 10 TIs from RGB imagery and 25 from multispectral data. All texture features were derived using a 3 × 3 sliding window to characterize fine-scale spatial heterogeneity. The GLCM was generated using the greycomatrix function in the Python scikit-image (skimage) library, and corresponding texture indices were obtained using the greycoprops function, as shown in Table A4 and Fig. 3c-Entropy_RGB.

Finally, feature groups were constructed using the datasets described above. Crop biomass prediction has evolved from approaches based solely on RGB-derived structural information to those incorporating multisensor data and diverse feature types (Bendig et al., 2014; Da et al., 2025b; Kim et al., 2018, 2023; Okada et al., 2024; Shen et al., 2025a). In this study, feature groups were constructed by combining RGB-based SIs with additional sensors and feature types to evaluate whether such multimodal approaches improve prediction performance for IPL soybean biomass estimation. In this naming

scheme, the prefix (before "–") denotes the sensor combination, while the suffix indicates the feature type. These groups included features using only structural information (RGB-SI); structural information combined with RGB-based vegetation indices (RGB-VI), texture indices (RGB-TI), and both (RGB-All); and structural information combined with RGB- and multispectral camera-based vegetation indices (RGB+MS-VI), texture indices (RGB+MS-TI), and both (RGB+MS-All). Feature engineering and model development were then performed separately for each feature group.IPL soybean biomass estimation model construction

2.3.5 Feature selection using recursive feature elimination

Recursive feature elimination (RFE) was applied for feature selection using four machine learning algorithms: support vector regression (SVR), random forest (RF), and eXtreme Gradient Boosting (XGB).

Initially, biomass prediction models were constructed using all available features with five-fold cross-validation for each algorithm. At each iteration, one feature was removed, the model was retrained, and the average R^2 score was recalculated using the reduced feature set. The feature associated with the lowest performance was permanently excluded, and the dataset was updated for the next iteration. This recursive process continued until only a single feature remained. Features were progressively eliminated, and the smallest feature subset achieving at least 99% of the maximum R^2 obtained during the RFE process was selected to reduce input dimensionality while maintaining comparable predictive performance. Here, the maximum R^2 refers to the highest predictive performance obtained among all evaluated feature subsets. (Shen et al., 2025a). Results for the RGB+MS-All feature group are illustrated in Fig. A2.

2.3.6 Machine learning model development through tree-structured parzen estimator

Models for predicting soybean biomass were developed using the calibration dataset and four machine learning architectures: SVR, RF, XGB, and a stacked ensemble model (SE) that integrated the four base learners. The SE employed multiple linear regression as a meta-model to combine predictions from the base models. Seventy percent of the dataset was allocated for training, and the remaining 30% was used for validation.

For each of the seven feature groups (RGB-SI, RGB-VI, RGB-TI, RGB-All, RGB+MS-VI, RGB+MS-TI, and RGB+MS-All), hyperparameter tuning for four machine learning architectures was performed using the feature subsets selected through RFE. Hyperparameter optimization used five-fold cross-validation combined with the Tree-structured Parzen Estimator (TPE). It enables efficient exploration of the search space by adaptively focusing on promising regions of the parameter domain. Specifically, the TPE algorithm iteratively partitioned the training dataset into five subsets, with one subset used for validation and the remaining four for training in each round. The hyperparameter configuration that achieved the highest average performance was selected to reduce overfitting.

2.3.7 Biomass estimation framework performance evaluation

The performance of biomass estimation was evaluated using the 2025 test dataset. Evaluation metrics for biomass estimation included the coefficient of determination (R^2), root mean square error (RMSE), and relative RMSE (rRMSE), calculated between predicted and measured biomass values.

To interpret the characteristics of the feature combinations and model architectures that achieved the highest performance in each feature group on the test dataset, SHapley Additive exPlanations (SHAP) analysis was conducted for the best-performing model in each group. SHAP analysis

quantified the contribution of each feature to model predictions while accounting for feature interactions (Lundberg et al., n.d.).

3 Results

3.1 Biomass data distribution across season and cultivar

The distribution of IPL soybean biomass across growing seasons is shown in Fig. 5 using kernel density estimation (KDE). In 2025, the proportion of samples with biomass values greater than 300 g for the cultivar *Gwanak1* was higher than that observed in 2024. This difference is likely attributable to more favorable growing conditions in 2025, as both temperature and rainfall were higher during the sampling period. In addition, the cultivar *Seonyu2ho* exhibited lower biomass values than *Gwanak1* under the same cultivation conditions, which appears to be associated with its earlier flowering stage.

As a result, the calibration and test datasets differed in both environmental conditions and cultivar composition, which led to distinct biomass distributions. These datasets are therefore suitable for evaluating model reproducibility under varying environmental conditions and assessing generalization to cultivars with different growth characteristics.

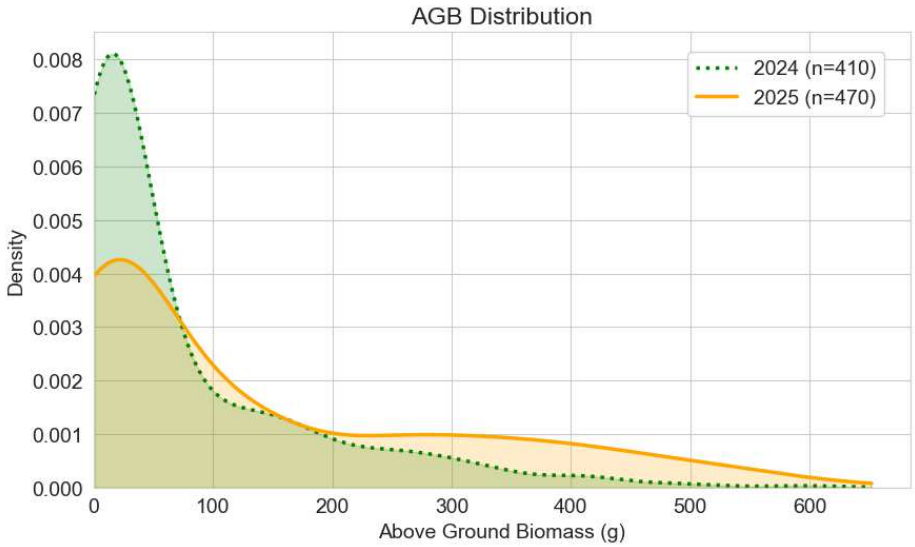


Fig. 5. Distribution of biomass samples across seasons and cultivars. The biomass distributions of the calibration and test datasets differ across seasons and cultivars, indicating that the datasets represent distinct environmental and varietal conditions and are therefore suitable for evaluating model generalization.

3.2 Performance of feature-driven machine learning framework across feature groups and model architectures

Biomass prediction performance was strongly influenced by feature composition and model architecture (Table 1). Among all feature groups, the highest prediction accuracy was achieved using the RGB+MS-All combination, particularly with the SVR model (R^2 = 0.89, RMSE = 53.15 g, and rRMSE = 8.50%). This finding suggests that integrating structural, spectral, and textural information derived from multisource UAV imagery provides the most comprehensive representation of IPL soybean biomass.

Within RGB-only feature groups, SIs (RGB-SI) provided relatively strong predictive performance ($R^2 \leq 0.73$), confirming that canopy-scale SIs play a fundamental role in biomass estimation. The addition of VIs (RGB-VI) or texture features (RGB-TI) resulted in marginal improvements or reduced

performance in some cases. However, the scatterplots of the best-performing model for each feature group as shown in Fig. 6 highlight the limitations of RGB-based features. Predictions tended to saturate at higher biomass levels, showing pronounced underestimation and deviation from the 1:1 line. This saturation effect indicates that RGB-derived features, particularly structural and visible-range indices, have limited sensitivity to biomass variability under dense canopy conditions. Conversely, feature groups incorporating multispectral data (RGB+MS-VI and RGB+MS-All) substantially reduced this saturation effect. The corresponding scatterplots displayed tighter clustering around the 1:1 line and improved prediction accuracy across the overall biomass range, particularly at higher values.

Regarding model architecture, SVR consistently demonstrated the most stable and highest predictive performance across feature groups, particularly in test datasets. In contrast, RF, XGB, and SE showed strong calibration performance but reduced generalization ability. For example, XGB achieved high calibration R^2 values (≤ 0.99), while its test performance dropped substantially across several feature groups (e.g., RGB-VI: $R^2 = 0.52$; RGB-All: $R^2 = 0.57$), indicating overfitting. RF showed more stable but lower performance across feature groups ($R^2 \approx 0.69$–0.85).

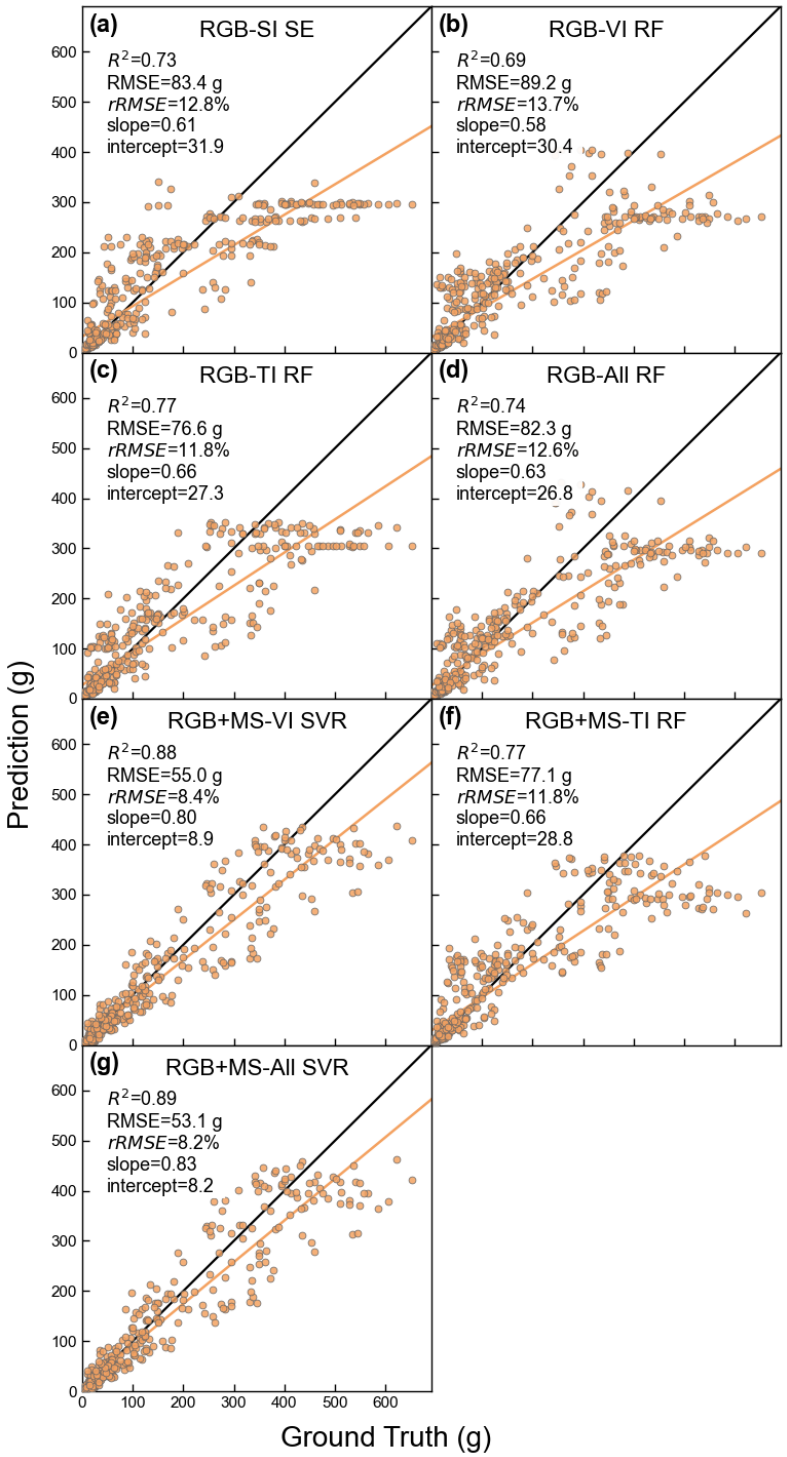
These findings indicate that optimal IPL biomass estimation can be achieved by combining multisource UAV-derived features with relatively simple and stable ML architectures. The integration of RGB and multispectral data improves sensitivity to physiological variability and mitigates saturation effects, while SVR ensures robust generalization across diverse cultivation environments.

Table 1. Model performance results across feature combinations and machine learning architectures, including R^2, RMSE, and rRMSE.

Feature Group	Models	R^2	RMSE (g)	rRMSE (%)

		calibration	test	calibration	test	calibration	test
RGB-SI	SVR	0.86	0.69	25.8	90.5	7.6	13.9
	RF	0.87	0.60	24.8	101.7	7.3	15.6
	XGB	0.88	0.72	23.7	85.7	7.0	13.2
	SE	0.86	**0.73**	26.1	**83.4**	7.6	**12.8**
RGB-VI	SVR	0.85	0.68	27.0	90.7	7.9	13.9
	RF	0.97	**0.69**	12.9	**89.2**	3.8	**13.7**
	XGB	0.98	0.52	8.5	112.2	2.5	17.2
	SE	0.99	0.48	7.3	116.6	2.1	17.9
RGB-TI	SVR	0.85	0.76	26.5	79.3	7.8	12.2
	RF	0.89	**0.77**	23.3	**76.6**	6.8	**11.8**
	XGB	0.95	0.73	15.6	83.2	4.6	12.8
	SE	0.95	0.73	15.4	83.4	4.5	12.8
RGB-All	SVR	0.85	0.71	26.5	87.6	7.8	13.4
	RF	0.97	**0.74**	12.2	**82.3**	3.6	**12.6**
	XGB	0.98	0.57	9.2	105.3	2.7	16.2
	SE	0.99	0.51	7.9	112.4	2.3	17.3
RGB+MS-VI	SVR	0.88	**0.88**	25.6	**55.0**	7.5	**8.4**
	RF	0.94	0.84	17.3	65.3	5.1	10.0
	XGB	0.98	0.83	10.5	66.8	3.1	10.3
	SE	0.98	0.82	9.9	68.1	2.9	10.5
RGB+MS-TI	SVR	0.86	0.73	25.4	83.9	7.4	12.9
	RF	0.93	**0.77**	18.8	**77.1**	5.5	**11.8**
	XGB	0.96	0.67	13.4	92.2	3.9	14.2
	SE	0.96	0.66	13.1	93.5	3.9	14.4
RGB+MS-All	SVR	0.89	**0.89**	25.8	**53.2**	7.6	**8.5**
	RF	0.94	0.85	17.4	61.3	5.5	9.7
	XGB	0.99	0.81	6.4	70.8	4.0	10.9
	SE	0.99	0.79	5.1	74.0	4.0	11.4

488
489


(a) RGB-SI SE
R^2=0.73
RMSE=83.4 g
rRMSE=12.8%
slope=0.61
intercept=31.9
(b) RGB-VI RF
R^2=0.69
RMSE=89.2 g
rRMSE=13.7%
slope=0.58
intercept=30.4
(c) RGB-TI RF
R^2=0.77
RMSE=76.6 g
rRMSE=11.8%
slope=0.66
intercept=27.3
(d) RGB-All RF
R^2=0.74
RMSE=82.3 g
rRMSE=12.6%
slope=0.63
intercept=26.8
(e) RGB+MS-VI SVR
R^2=0.88
RMSE=55.0 g
rRMSE=8.4%
slope=0.80
intercept=8.9
(f) RGB+MS-TI RF
R^2=0.77
RMSE=77.1 g
rRMSE=11.8%
slope=0.66
intercept=28.8
(g) RGB+MS-All SVR
R^2=0.89
RMSE=53.1 g
rRMSE=8.2%
slope=0.83
intercept=8.2
Prediction (g)
Ground Truth (g)
0
100
200
300
400
500
600

490

Fig. 6. Scatterplots of predicted versus ground truth biomass for the best-performing model in each feature group. The best models for each feature group were as follows: RGB-SI (SE), RGB-VI (RF), RGB-TI (RF), RGB-All (RF), RGB+MS-VI (SVR), RGB+MS-TI (RF), and RGB+MS-All (SVR). The solid black line represents the 1:1 relationship, and the orange line indicates the fitted regression line. RGB-based feature groups exhibit saturation effects at higher biomass levels, whereas multisource feature combinations (RGB+MS) reduce saturation and improve prediction accuracy across the overall biomass range.

3.3 Feature selection and interpretation for individual plant-level soybean biomass using SHAP analysis

Fig. 7 presents the RGB+MS-All configuration as a representative example, while the selected features and corresponding SHAP results for the RGB-SI, RGB-VI, RGB-TI, RGB-All, RGB+MS-VI, and RGB+MS-TI combinations are provided in the Appendix (Fig. A3–A8).

Red-edge and NIR-based VIs, particularly RECI and NDRE, contributed dominantly to the model predictions. These indices are highly sensitive to leaf chlorophyll concentration and canopy nitrogen status, which directly regulate photosynthetic capacity and biomass accumulation (Barboza et al., 2023; Hamada et al., 2023). Compared with visible-range indices, red-edge and NIR features provide greater sensitivity under high leaf-area conditions, enabling more reliable characterization of dense-canopy variability for biomass prediction. As expected, the morphological feature PH × VF consistently showed strong contributions. SHAP analysis revealed that this interaction term exerted one of the strongest influences on biomass prediction, confirming its importance as a structural variable that integrates canopy height and vegetation fraction (Kim et al., 2018, 2023). Most texture features were excluded during the RFE process, indicating their relatively limited contribution to biomass prediction.

These findings indicate that biomass estimation is influenced not only by physiological traits but also by the physical structure of the canopy. SIs primarily capture canopy scale, whereas VIs, particularly those incorporating NIR and red-edge bands, represent photosynthetic capacity and internal leaf properties. Therefore, multispectral features provide enhanced sensitivity to plant physiological conditions beyond what is achievable with RGB data alone. The integration of these complementary feature types enables a more comprehensive representation of biomass variability at the IPL.

Meanwhile, SHAP values derived from the Stacked Ensemble model showed that the XGB base learner contributed most substantially to the final ensemble predictions. This pattern was consistent across feature sets, suggesting that the ensemble output was largely driven by the XGB component and therefore exhibited prediction behavior similar to that of XGB as shown in Table 1.

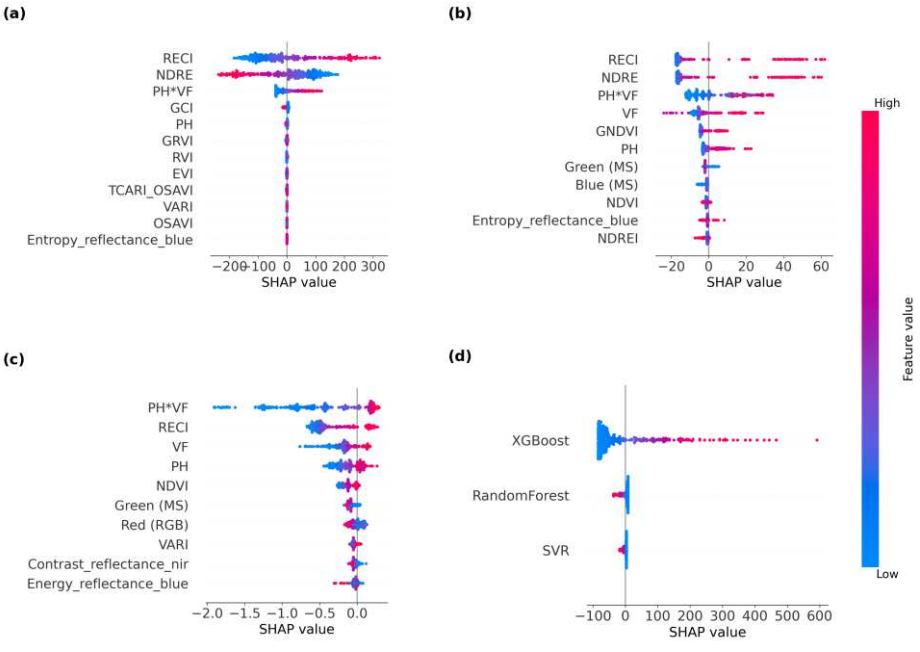


Fig. 7. Bee swarm plots of SHAP values presenting RGB+MS-All feature contributions across various machine learning models: (a) SVR, (b) RF, (c) XGB, and (d) SE. Each point represents an individual sample used in the model evaluation. The color gradient ranging from blue to red reflects increasing values of the target variable, soybean biomass. Features with higher absolute SHAP values indicate a stronger influence on the model's prediction.

3.4 Individual plant-level-based soybean biomass mapping and spatial variability analysis

Biomass is a key growth indicator associated with photosynthetic activity supporting reproductive development after flowering. Fig. 8a presents the IPL biomass map generated from UAV RGB and multispectral images acquired at the flowering stage (July 25, 2025). The generated IPL biomass maps were converted to the plot level using rectangular ROIs with a width of 2 m and spanning four crop rows, following Da et al., (2025), where five samples were randomly selected within each ROI to compute mean biomass values (Fig. 8b). In addition, kriging interpolation was applied to generate continuous spatial surfaces using Surfer 13 (Golden Software, USA).

Within the same field, the number of data points decreased from 2,704 at the IPL to 122 at the plot level, resulting in a substantial reduction in data density. Spatial resolution, defined as the average distance between adjacent data points, decreased from 0.25 m to 1.9 m. Aggregation at the plot level produced a biomass map with reduced spatial variability, characterized by a narrower variance range, attenuation of local extrema, and a diminished ability to resolve fine-scale crop variability (Fig. 8). The semivariogram for IPL data showed a larger nugget and higher semivariance, reflecting strong plant-to-plant variability, whereas the plot-level semivariogram exhibited a smaller nugget and steeper increase, indicating reduced local variability and clearer spatial gradients. (Fig. A9). These results highlight a key limitation of plot-level analysis in capturing intra-field heterogeneity, whereas UAV-based

IPL mapping enables the acquisition of high-resolution, large-volume phenotypic data within field breeding.

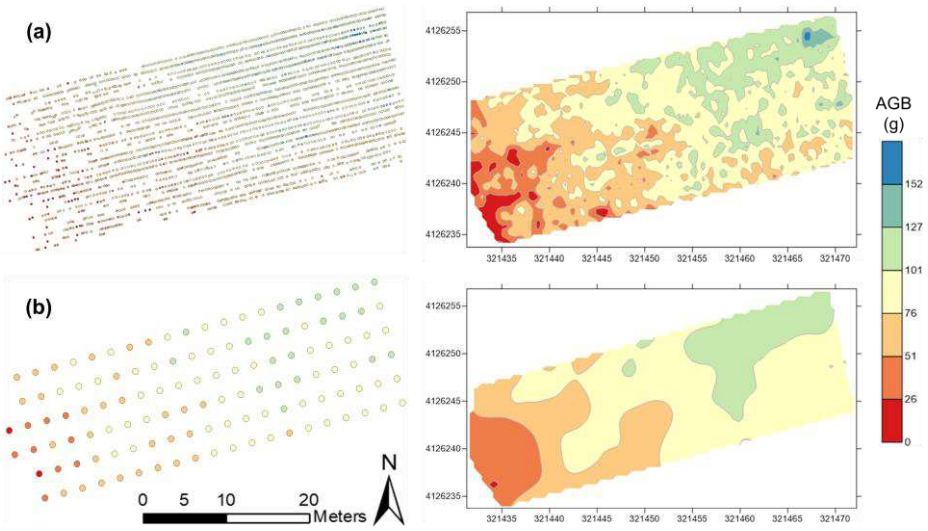


Fig. 8. UAV-based soybean biomass maps (a) at the individual plant level and (b) plot level, along with their corresponding kriging interpolation maps at the flowering stage (July 25, 2025). A distinct spatial pattern is observed, with lower biomass in the southwestern region.

The kriging and semivariogram analyses revealed clear biomass heterogeneity within the field, with lower biomass and reduced crop establishment in the southwestern region, as indicated by spatial gradients in the kriging maps and by increasing semivariance with lag distance. Two main factors likely explain this pattern: drainage and sowing quality. The water drainage inlet is located in the southwestern area, where insufficient drainage capacity likely prevented discharge during rainfall, leading to water accumulation and resulting in excess moisture stress. (Fig. 9). In addition, during west-to-east sowing, the seeding unit was operated independently from the tillage and ridge-forming components, making consistent depth control

difficult. As seeding conditions were gradually adjusted based on real-time feedback during operation, the western sections, where sowing was initiated, tended to exhibit less stable conditions, while conditions improved toward the east. Consequently, plant establishment was reduced in the southwestern region.

These findings confirm that the proposed UAV-based IPL biomass mapping effectively captures stable spatial variability and localized disturbances associated with agricultural management practices. By enabling the identification of such environmental and human-induced effects, this approach supports more reliable phenotyping and highlights its potential as an high-throughput phenotyping tool for breeding and precision agriculture applications.



Fig. 9. Digital terrain model (DTM) of the study field. The highlighted area (red box) shows water accumulation after rainfall due to inadequate drainage at the inlet, as confirmed by the corresponding RGB image.

3.5 Individual plant-level soybean biomass time series dynamic for high-throughput phenotyping

To further investigate temporal biomass dynamics, the soybean cultivar *Gwanak1* was evaluated via the selection of approximately 30 high-yielding and 30 low-yielding individual plants at harvest. These plants were grouped accordingly, and their biomass trajectories over time were analyzed (Fig. 10).

The results revealed distinct differences in biomass accumulation between the two groups across growth stages. During the early vegetative stage, biomass increased gradually, but differences between high- and low-yielding groups remained relatively small and inconsistent, indicating that early-stage biomass does not fully reflect final yield potential. Conversely, post-flowering, biomass increased markedly, and the divergence between the groups became pronounced.

This transition is consistent with the spatial analysis results (Section 3.5), where distinct spatial patterns emerged post-flowering. Similarly, at the IPL, biomass differences between high- and low-yielding plants became more pronounced and stable post-flowering, suggesting that post-flowering biomass better represents intrinsic growth performance and yield potential. Rapid biomass accumulation during the reproductive stage is likely associated with active pod development and seed filling under favorable environmental conditions, including sufficient temperature and rainfall.

In particular, the high-yielding group consistently accumulated more biomass than the low-yielding group, with differences becoming increasingly evident during the reproductive stage. This pattern indicates that post-flowering biomass development plays a critical role in determining final yield potential.

From a breeding perspective, temporal biomass dynamics are important because they reflect differences in growth efficiency, resource allocation, and reproductive development among individual plants (Masino et al., 2018). Monitoring these dynamics at the IPL provides valuable insights into genotype performance and yield formation processes. UAV-based IPL biomass mapping enabled the identification and temporal tracking of these differences, demonstrating its potential as an effective phenotyping tool in breeding programs.

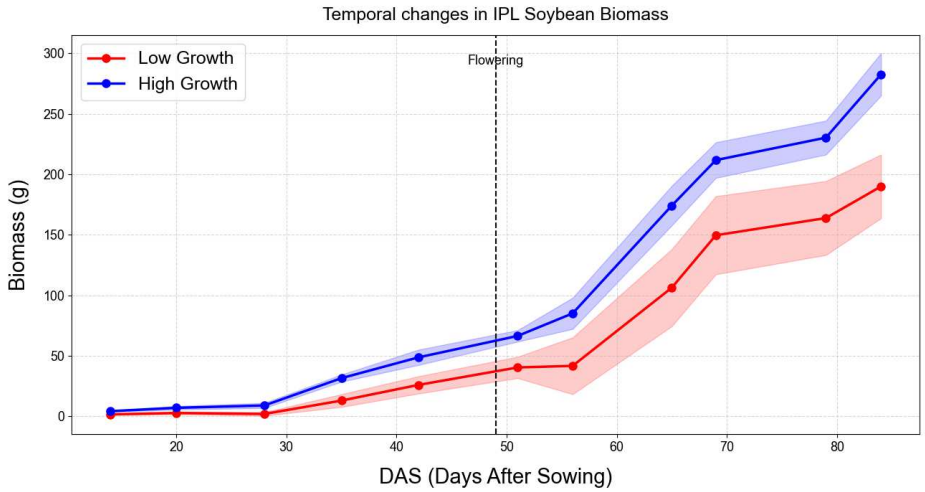


Fig. 10. Temporal biomass time series dynamics of high- and low-yielding soybean plants (*Gwanak1*) across growth stages. The blue and red lines represent the biomass of high- and low-yielding groups, respectively, and the shaded areas indicate the variability (± 1 standard deviation) within each group. The vertical dashed line denotes the flowering stage.

4 Discussion

This study demonstrated that a feature-driven machine learning framework based on UAV imagery can accurately predict soybean above-ground biomass (AGB) at the individual plant level (IPL). The results confirmed that, similar

to the most previous studies conducted at the plot level (Da et al., 2025a; Okada et al., 2024; Ranđelović et al., 2023), biomass estimation using feature selection and machine learning models was also feasible at the IPL. However, the comparative analysis in this study (Fig. 8) revealed that plot-based approaches are inherently less effective in capturing plant-level variability, limiting their applicability to precision agriculture and high-throughput phenotyping requiring high-resolution spatial data.

IPL-based analysis offers several important benefits for crop monitoring and phenotyping applications. First, it enables the acquisition of a large number of samples within a limited field area, which is particularly beneficial for high-throughput phenotyping in breeding programs (Gill et al., 2022; Roth et al., 2025; Tanaka et al., 2024; Xu & Li, 2022). Second, it allows the analysis of fine-scale spatial variability, making it possible to detect subtle environmental heterogeneity that may occur even within short distances (Masino et al., 2018; Toriyama, 2020). Third, it provides direct measurements at the IPL, avoiding the smoothing effects caused by spatial aggregation, thereby improving data precision (section 3.4). These advantages highlight the potential of IPL-based approaches as a powerful tool for both precision agriculture and plant phenotyping applications.

A notable finding of this study is that texture indices (TIs) did not exhibit significant importance in biomass prediction at the IPL. In previous studies conducted at the plot level (Da et al., 2025a; Shen et al., 2025b), TIs have been shown to capture spatial patterns such as gaps among canopy stand, which indirectly reflect crop growth conditions. However, in the IPL context, where each sample corresponds to a single plant, such spatial variability is inherently limited. As a result, TI-derived features primarily represent the arrangement of leaves within an individual canopy, providing minimal additional information for biomass estimation. In contrast, structural features such as plant height (PH) and vegetation fraction (VF), along with vegetation

679 indices (VIs) related to chlorophyll content, showed high importance. In
680 particular, red-edge and near-infrared (NIR)-based indices, such as RECI and
681 NDRE, were identified as dominant predictors, likely due to their reduced
682 saturation and strong sensitivity to physiological traits associated with
683 biomass accumulation (Qiao et al., 2022; Xie et al., 2018).
684 Another key strength of this study lies in its experimental design. Model
685 development and evaluation were conducted using datasets collected from
686 different years and different fields, enabling a rigorous assessment of model
687 generalizability. In contrast, many previous studies, although separating
688 training and test datasets, relied on data collected under similar environmental
689 conditions, which may overestimate model performance (Biswal et al., 2024b;
690 Liu et al., 2022, 2025). Under the more challenging conditions adopted in this
691 study, Stacked Ensemble model did not achieve superior performance. While
692 these models exhibited strong fitting ability during calibration, their
693 performance decreased on independent test datasets, indicating overfitting.
694 Interestingly, the support vector regressor (SVR) with a linear kernel
695 showed relatively lower performance during calibration but outperformed
696 more complex models in the test phase. This result suggests that, under
697 conditions where the distribution of training and test data differs, simpler and
698 more stable models may provide better generalization than highly flexible,
699 nonlinear architectures. Given the limited availability of agricultural data and
700 the increasing variability of environmental conditions, prioritizing model
701 robustness over fitting complexity appears to be a more effective strategy for
702 practical applications.
703 Despite the promising results, several limitations should be acknowledged.
704 In this study, two separate UAV flights were required to acquire high-
705 resolution RGB imagery and multispectral imagery, respectively, which
706 increases operational complexity and reduces acquisition efficiency. In
707 addition, the independent acquisition of the two datasets may introduce slight

spatial inconsistencies caused by canopy movement or environmental variation between flights (Nguyen et al., 2025). Future studies should explore UAV platforms capable of simultaneously acquiring high-resolution RGB and multispectral data within a single flight (Maimaitijiang et al., 2020). Although biomass prediction at the IPL was successfully achieved, the current workflow still relies on manual processes for IPL region definition and crop delineation. This dependency limits scalability and practical applicability. Developing automated IPL mapping frameworks that can robustly handle complex canopy structures, including overlapping plants, will be essential for translating model outputs into practical breeding and field management applications.

5 Conclusion

In this study, a UAV-based multisource feature-driven ML framework for estimating soybean biomass at IPL was developed and validated. Multisource UAV imagery, including RGB and multispectral data, was collected across two growing seasons under independent field conditions, and structural, spectral, and textural features were extracted from IPL-defined crop regions to construct biomass prediction models.

The results showed that biomass prediction performance was strongly dependent on feature composition and model architecture. Among all combinations, the SVR model using integrated RGB and multispectral features (RGB+MS-All) achieved the highest accuracy (R^2 = 0.89, RMSE = 53.15 g, and rRMSE = 8.50%) on the independent test dataset. These findings indicate that combining multisource UAV features with relatively simple and stable models is more effective for robust biomass estimation with limited agricultural datasets.

Overall, this study confirms the feasibility of UAV-based IPL soybean biomass estimation as an HTP tool. The proposed framework enables accurate, non-destructive, and spatially explicit biomass quantification at the IPL. Beyond prediction accuracy, it provides spatial mapping and temporal analysis of biomass dynamics, revealing spatial variability associated with environmental conditions and human management, as well as distinct post-flowering growth differences between high- and low-yielding plants. These capabilities highlight its potential for crop monitoring, breeding selection, and precision agriculture applications.

Funding

This work was supported by the LS Mtron–SNU CALS Digital Agriculture Industry-Academia Collaboration Project (Grant No. 500-20231078).

References

Ali, J., Haoran, W., Mehmood, K., Hussain, W., Iftikhar, F., Shahzad, F., Hussain, K., Qun, Y., & Zhongkui, J. (2025). Remote sensing and integration of machine learning algorithms for above-ground biomass estimation in Larix principis-rupprechtii Mayr plantations: a case study using Sentinel-2 and Landsat-9 data in northern China. *Frontiers in Environmental Science*, *13*. https://doi.org/10.3389/fenvs.2025.1577298

Alsajri, F. A., Wijewardana, C., Krutz, L. J., Irby, J. T., Golden, B., & Reddy, K. R. (2019). Quantifying and Validating Soybean Seed Emergence Model as a Function of Temperature. *American Journal of Plant Sciences*, *10*(01), 111–124. https://doi.org/10.4236/ajps.2019.101010

Barboza, T. O. C., Ardigueri, M., Souza, G. F. C., Ferraz, M. A. J., Gaudencio, J. R. F., & Santos, A. F. dos. (2023). Performance of Vegetation Indices to Estimate Green Biomass Accumulation in Common Bean. *AgriEngineering*, *5*(2), 840–854. https://doi.org/10.3390/agriengineering5020052

Bendig, J., Bolten, A., Bennertz, S., Broscheit, J., Eichfuss, S., & Bareth, G. (2014). Estimating biomass of barley using crop surface models (CSMs) derived from UAV-based RGB imaging. *Remote Sensing*, *6*(11), 10395–10412. https://doi.org/10.3390/rs61110395

766 Biswal, S., Pathak, N., Chatterjee, C., & Mailapalli, D. R. (2024a). Estimation
767 of aboveground biomass from spectral and textural characteristics of
768 paddy crop using UAV-multispectral images and machine learning
769 techniques. *Geocarto International*, *39*(1).
770 https://doi.org/10.1080/10106049.2024.2364725
771 Biswal, S., Pathak, N., Chatterjee, C., & Mailapalli, D. R. (2024b). Estimation
772 of aboveground biomass from spectral and textural characteristics of
773 paddy crop using UAV-multispectral images and machine learning
774 techniques. *Geocarto International*, *39*(1).
775 https://doi.org/10.1080/10106049.2024.2364725
776 Da, H., Li, Y., Xu, L., Wang, S., Hu, L., Hu, Z., Wei, Q., Zhu, R., Chen, Q.,
777 Xin, D., & Zhao, Z. (2025a). Advancing soybean biomass estimation
778 through multi-source UAV data fusion and machine learning algorithms.
779 *Smart Agricultural Technology*, *10*.
780 https://doi.org/10.1016/j.atech.2025.100778
781 Da, H., Li, Y., Xu, L., Wang, S., Hu, L., Hu, Z., Wei, Q., Zhu, R., Chen, Q.,
782 Xin, D., & Zhao, Z. (2025b). Advancing soybean biomass estimation
783 through multi-source UAV data fusion and machine learning algorithms.
784 *Smart Agricultural Technology*, *10*.
785 https://doi.org/10.1016/j.atech.2025.100778
786 Gill, T., Gill, S. K., Saini, D. K., Chopra, Y., de Koff, J. P., & Sandhu, K. S.
787 (2022). A Comprehensive Review of High Throughput Phenotyping and
788 Machine Learning for Plant Stress Phenotyping. In *Phenomics* (Vol. 2,
789 Number 3, pp. 156–183). Springer. https://doi.org/10.1007/s43657-022-
790 00048-z
791 Hamada, Y., Zumpf, C. R., Quinn, J. J., & Negri, M. C. (2023). Estimating
792 Field-Level Perennial Bioenergy Grass Biomass Yields Using the
793 Normalized Difference Red-Edge Index and Linear Regression Analysis
794 for Central Virginia, USA. *Energies*, *16*(21).
795 https://doi.org/10.3390/en16217397
796 Hartman, G. L., West, E. D., & Herman, T. K. (2011). Crops that feed the World
797 2. Soybean-worldwide production, use, and constraints caused by
798 pathogens and pests. *Food Security*, *3*(1), 5–17.
799 https://doi.org/10.1007/s12571-010-0108-x
800 Hsiao, T. C., Heng, L., Steduto, P., Rojas-Lara, B., Raes, D., & Fereres, E.
801 (2009). Aquacrop-The FAO crop model to simulate yield response to
802 water: III. Parameterization and testing for maize. *Agronomy Journal*,
803 *101*(3), 448–459. https://doi.org/10.2134/agronj2008.0218s
804 Huang, J., Sedano, F., Huang, Y., Ma, H., Li, X., Liang, S., Tian, L., Zhang,
805 X., Fan, J., & Wu, W. (2016). Assimilating a synthetic Kalman filter leaf
806 area index series into the WOFOST model to improve regional winter
807 wheat yield estimation. *Agricultural and Forest Meteorology*, *216*, 188–
808 202. https://doi.org/10.1016/j.agrformet.2015.10.013

Jang, G. J., Kim, J., Yu, J. K., Kim, H. J., Kim, Y., Kim, D. W., Kim, K. H., Lee, C. W., & Chung, Y. S. (2020). Review: Cost-effective unmanned aerial vehicle (UAV) platform for field plant breeding application. In *Remote Sensing* (Vol. 12, Number 6). MDPI AG. https://doi.org/10.3390/rs12060998

Kim, D. W., Jeong, S. J., Lee, W. S., Yun, H., Chung, Y. S., Kwon, Y. S., & Kim, H. J. (2023). Growth monitoring of field-grown onion and garlic by CIE L*a*b* color space and region-based crop segmentation of UAV RGB images. *Precision Agriculture*, *24*(5), 1982–2001. https://doi.org/10.1007/s11119-023-10026-8

Kim, D. W., Yun, H. S., Jeong, S. J., Kwon, Y. S., Kim, S. G., Lee, W. S., & Kim, H. J. (2018). Modeling and testing of growth status for Chinese cabbage and white radish with UAV-based RGB imagery. *Remote Sensing*, *10*(4). https://doi.org/10.3390/rs10040563

Kouadio, L., El Jarroudi, M., Belabess, Z., Laasli, S. E., Roni, M. Z. K., Amine, I. D. I., Mokhtari, N., Mokrini, F., Junk, J., & Lahlali, R. (2023). A Review on UAV-Based Applications for Plant Disease Detection and Monitoring. In *Remote Sensing* (Vol. 15, Number 17). Multidisciplinary Digital Publishing Institute (MDPI). https://doi.org/10.3390/rs15174273

LANCASHIRE, P. D., BLEIHOLDER, H., BOOM, T. VAN DEN, LANGELÜDDEKE, P., STAUSS, R., WEBER, E., & WITZENBERGER, A. (1991). A uniform decimal code for growth stages of crops and weeds. *Annals of Applied Biology*, *119*(3), 561–601. https://doi.org/10.1111/j.1744-7348.1991.tb04895.x

Liu, Y., Fan, Y., Yue, J., Ma, Y., Yang, F., Fan, J., Chen, R., Bian, M., & Feng, H. (2025). UAV-based remote sensing estimation of above-ground biomass in different crops: A review. In *International Journal of Applied Earth Observation and Geoinformation* (Vol. 144). Elsevier B.V. https://doi.org/10.1016/j.jag.2025.104938

Liu, Y., Feng, H., Yue, J., Fan, Y., Jin, X., Song, X., Yang, H., & Yang, G. (2022). Estimation of Potato Above-Ground Biomass Based on Vegetation Indices and Green-Edge Parameters Obtained from UAVs. *Remote Sensing*, *14*(21). https://doi.org/10.3390/rs14215323

López-García, S. L., Vázquez, T. E. E., Favelukes, G., & Lodeiro, A. R. (2002). Rhizobial position as a main determinant in the problem of competition for nodulation in soybean. *Environmental Microbiology*, *4*(4), 216–224. https://doi.org/10.1046/j.1462-2920.2002.00287.x

Lundberg, S. M., Allen, P. G., & Lee, S.-I. (n.d.). *A Unified Approach to Interpreting Model Predictions*. Retrieved https://github.com/slundberg/shap

Maimaitijiang, M., Sagan, V., Sidike, P., Hartling, S., Esposito, F., & Fritschi, F. B. (2020). Soybean yield prediction from UAV using multimodal data

fusion and deep learning. *Remote Sensing of Environment*, *237*. https://doi.org/10.1016/j.rse.2019.111599

Malashin, I., Tynchenko, V., Gantimurov, A., Nelyub, V., Borodulin, A., & Tynchenko, Y. (2024). Predicting Sustainable Crop Yields: Deep Learning and Explainable AI Tools. *Sustainability (Switzerland)*, *16*(21). https://doi.org/10.3390/su16219437

Mall, R. K., Lal, M., Bhatia, V. S., Rathore, L. S., & Singh, R. (2004). Mitigating climate change impact on soybean productivity in India: A simulation study. *Agricultural and Forest Meteorology*, *121*(1–2), 113–125. https://doi.org/10.1016/S0168-1923(03)00157-6

Masino, A., Rugeroni, P., Borrás, L., & Rotundo, J. L. (2018). Spatial and temporal plant-to-plant variability effects on soybean yield. *European Journal of Agronomy*, *98*, 14–24. https://doi.org/10.1016/j.eja.2018.02.006

Matyukira, C., & Mhangara, P. (2024). Utilising RGB drone imagery and vegetation indices for accurate above-ground biomass estimation: a case study of the cradle nature reserve, Gauteng Province, South Africa. *Geocarto International*, *39*(1). https://doi.org/10.1080/10106049.2024.2390512

Nguyen, V. H., Le, C. D., Truong, M. T., Bui, M. P. T., & Le, T. P. (2025). A dataset of aligned RGB and multispectral UAV imagery for semantic segmentation of weedy rice. *Data in Brief*, *63*. https://doi.org/10.1016/j.dib.2025.112237

Oerke, E. C. (2006). Crop losses to pests. In *Journal of Agricultural Science* (Vol. 144, Number 1, pp. 31–43). https://doi.org/10.1017/S0021859605005708

Okada, M., Barras, C., Toda, Y., Hamazaki, K., Ohmori, Y., Yamasaki, Y., Takahashi, H., Takanashi, H., Tsuda, M., Hirai, M. Y., Tsujimoto, H., Kaga, A., Nakazono, M., Fujiwara, T., & Iwata, H. (2024). High-Throughput Phenotyping of Soybean Biomass: Conventional Trait Estimation and Novel Latent Feature Extraction Using UAV Remote Sensing and Deep Learning Models. *Plant Phenomics*, *6*. https://doi.org/10.34133/plantphenomics.0244

Purcell, L. C., Ball, R. A., Reaper, J. D., & Vories, E. D. (2002). Radiation use efficiency and biomass production in soybean at different plant population densities. *Crop Science*, *42*(1), 172–177. https://doi.org/10.2135/cropsci2002.1720

Qiao, L., Tang, W., Gao, D., Zhao, R., An, L., Li, M., Sun, H., & Song, D. (2022). UAV-based chlorophyll content estimation by evaluating vegetation index responses under different crop coverages. *Computers and Electronics in Agriculture*, *196*. https://doi.org/10.1016/j.compag.2022.106775

Ranđelović, P., Đorđević, V., Miladinović, J., Prodanović, S., Ćeran, M., & Vollmann, J. (2023). High-throughput phenotyping for non-destructive estimation of soybean fresh biomass using a machine learning model and temporal UAV data. *Plant Methods*, *19*(1). https://doi.org/10.1186/s13007-023-01054-6

Roth, L., Marzougui, A., & Walter, A. (2025). A review of the journey of field crop phenotyping: From trait stamp collections and fancy robots to phenomics-informed crop performance predictions. In *Journal of Plant Physiology* (Vol. 311). Elsevier GmbH. https://doi.org/10.1016/j.jplph.2025.154542

Shammi, S. A., Huang, Y., Xie, W., Feng, G., Tewolde, H., Zhang, X., Jenkins, J., & Shankle, M. (2025). Modeling and Estimating Soybean Leaf Area Index and Biomass Using Machine Learning Based on Unmanned Aerial Vehicle-Captured Multispectral Images. *Phyton-International Journal of Experimental Botany*, *94*(9), 2745–2766. https://doi.org/10.32604/phyton.2025.068955

Shen, S., Li, W., Zou, J., Harrison, M. T., Liu, S., Eyshi Rezaei, E., Liu, K., Kamali, B., Wang, Z., Zhang, D., Zheng, A., Chen, F., & Yin, X. (2025a). Fusing UAV multiple data and phenology to predict crop biomass. *Information Processing in Agriculture*. https://doi.org/10.1016/j.inpa.2025.09.001

Shen, S., Li, W., Zou, J., Harrison, M. T., Liu, S., Eyshi Rezaei, E., Liu, K., Kamali, B., Wang, Z., Zhang, D., Zheng, A., Chen, F., & Yin, X. (2025b). Fusing UAV multiple data and phenology to predict crop biomass. *Information Processing in Agriculture*. https://doi.org/10.1016/j.inpa.2025.09.001

Tanaka, T. S. T., Wang, S., Jørgensen, J. R., Gentili, M., Vidal, A. Z., Mortensen, A. K., Acharya, B. S., Beck, B. D., & Gislum, R. (2024). Review of Crop Phenotyping in Field Plot Experiments Using UAV-Mounted Sensors and Algorithms. In *Drones* (Vol. 8, Number 6). Multidisciplinary Digital Publishing Institute (MDPI). https://doi.org/10.3390/drones8060212

Thomasz, E. O., Pérez-Franco, I., & García-García, A. (2024). Assessing the impact of climate change on soybean production in Argentina. *Climate Services*, *34*. https://doi.org/10.1016/j.cliser.2024.100458

Toriyama, K. (2020). Development of precision agriculture and ICT application thereof to manage spatial variability of crop growth. In *Soil Science and Plant Nutrition* (Vol. 66, Number 6, pp. 811–819). Taylor and Francis Ltd. https://doi.org/10.1080/00380768.2020.1791675

Ubbens, J., Cieslak, M., Prusinkiewicz, P., Parkin, I., Ebersbach, J., & Stavness, I. (2020). Latent space phenotyping: Automatic image-based phenotyping for treatment studies. *Plant Phenomics*, *2020*. https://doi.org/10.34133/2020/5801869

Wang, H., Singh, K. D., Poudel, H. P., Natarajan, M., Ravichandran, P., & Eisenreich, B. (2024). Forage Height and Above-Ground Biomass Estimation by Comparing UAV-Based Multispectral and RGB Imagery. *Sensors*, *24*(17). https://doi.org/10.3390/s24175794

Xie, Q., Dash, J., Huang, W., Peng, D., Qin, Q., Mortimer, H., Casa, R., Pignatti, S., Laneve, G., Pascucci, S., Dong, Y., & Ye, H. (2018). Vegetation Indices Combining the Red and Red-Edge Spectral Information for Leaf Area Index Retrieval. *IEEE Journal of Selected Topics in Applied Earth Observations and Remote Sensing*, *11*(5), 1482–1492. https://doi.org/10.1109/JSTARS.2018.2813281

Xu, R., & Li, C. (2022). A Review of High-Throughput Field Phenotyping Systems: Focusing on Ground Robots. In *Plant Phenomics* (Vol. 2022). American Association for the Advancement of Science. https://doi.org/10.34133/2022/9760269

Yang, Z., Qi, H., Hu, K., Kou, W., Xu, W., Wang, H., & Lu, N. (2025). Estimation of Amorphophallus Konjac Above-Ground Biomass by Integrating Spectral and Texture Information from Unmanned Aerial Vehicle-Based RGB Images. *Drones*, *9*(3). https://doi.org/10.3390/drones9030220

Ye, M., Wang, Z., Wu, M., Li, H., Gu, J., Yang, J., Zhang, H., & Zhang, Z. (2024). Optimized leaf anatomy improves photosynthetic producing capacity of mid-season indica rice in the Yangtze River Basin during the genetic improvement. *European Journal of Agronomy*, *158*. https://doi.org/10.1016/j.eja.2024.127196

Yun, H. S., Park, S. H., Kim, H.-J., Lee, W. D., Lee, K. Do, Hong, S. Y., & Jung, G. H. (2016). Use of Unmanned Aerial Vehicle for Multi-temporal Monitoring of Soybean Vegetation Fraction. *Journal of Biosystems Engineering*, *41*(2), 126–137. https://doi.org/10.5307/jbe.2016.41.2.126

Zambrano, P., Calderon, F., Villegas, H., Paillacho, J., Pazmino, D., & Realpe, M. (2023). UAV Remote Sensing applications and current trends in crop monitoring and diagnostics: A Systematic Literature Review. *2023 IEEE 13th International Conference on Pattern Recognition Systems, ICPRS 2023*. https://doi.org/10.1109/ICPRS58416.2023.10179038

Zhao, S., Zhao, X., & Li, Y. (2023). Relationship between the trait response of aboveground and belowground parts of dominant plant species to groundwater depth change in Horqin Sandy Land, eastern China. *Ecological Indicators*, *156*. https://doi.org/10.1016/j.ecolind.2023.111001

Zhu, Y., Fan, F., Zhang, Z., Yu, X., Jiang, T., Li, L., Liu, Y., Bai, Y., Tang, Z., Liu, S., Yin, D., & Jin, X. (2025). How to Better Use Canopy Height in Soybean Biomass Estimation. *Agriculture (Switzerland)*, *15*(10). https://doi.org/10.3390/agriculture15101024

979

Supplementary Files

This is a list of supplementary files associated with this preprint. Click to download.

- Appendix.docx
- image1.png